Switchable Primaries Using Shiftable Layers of Color Filter Arrays

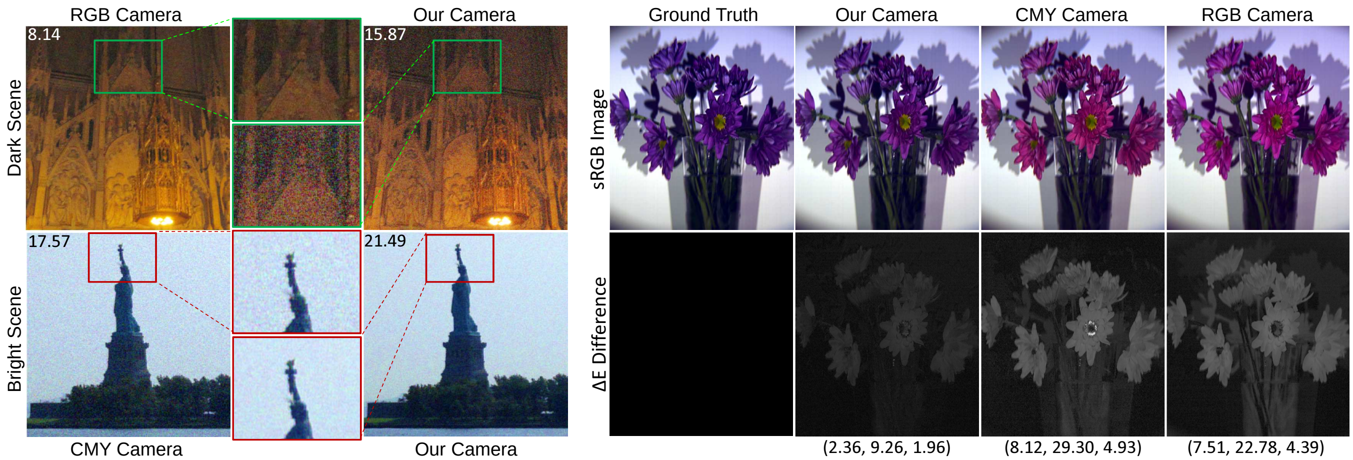

Figure 1: *Left: The CMY mode of our camera provides a superior SNR over a RGB camera when capturing a dark scene (top) and the RGB mode provides superior SNR over CMY camera when capturing a lighted scene. To demonstrate this, each image is marked with its quantitative SNR on the top left. Right: The RGBCY mode of our camera provides better color fidelity than a RGB or CMY camera for colorful scene (top). The ΔE deviation in CIELAB space of each of these images from a ground truth (captured using SOC-730 hyperspectral camera) is encoded as grayscale images with error statistics (mean, maximum and standard deviation) provided at the bottom of each image. Note the close match between the image captured with our camera and the ground truth.*

Abstract

We present a camera with switchable primaries using shiftable layers of color filter arrays (CFAs). By layering a pair of CMY CFAs in this novel manner, we can switch between multiple sets of color primaries (namely RGB, CMY and RGBCY) in the same camera. In contrast to having fixed color primaries (like RGB or CMY) which cannot provide optimal image quality for all scene conditions, our camera with switchable primaries provide optimal image quality in terms of *color fidelity* and *signal to noise ratio* for multiple scene conditions.

Next, we show that the same concept can be used to layer two RGB CFAs to design a camera that can switch between low dynamic range (LDR) and high dynamic range (HDR) modes. Further, we show that such layering of CFAs can be generalized as a constrained satisfaction problem (CSP) allowing us to constrain a large number of parameters (e.g. different operational modes, amount and direction of the shifts, placement of the primaries in the CFA) to provide an optimal solution.

We investigate several practical design options for shifting and layering of the CFAs. Finally, we demonstrate these by building prototype cameras for both switchable primaries and switchable LDR and HDR modes.

To the best of our knowledge, we present, for the first time, the concept of shiftable layers of CFAs that can provide a new degree of freedom in photography where multiple operational modes are available to the user in a single camera for optimizing the picture quality based on the nature of the scene geometry, color and illumination.

Keywords: computational photography, color filters, capture noise

1 Introduction

Camera consumers are forced to live with several trade-offs originating from conflicting demands on the quality. For example, broad-band filters (e.g. CMY), being more light efficient than narrow-band filters (e.g. RGB), are desired for scenes with low illumination (e.g. night/dark scenes). But, they have lower color fidelity. Further, demultiplexing RGB values from the captured CMY values can result in more noise in brighter scenes. Hence, narrow-band filters are desired for scenes with high illumination (e.g. daylight/bright scenes). However, since current cameras come with fixed RGB or CMY color filter arrays or CFAs, users have to accept sub-optimal image quality either for dark or bright scenes. Similarly, faithful capture of colorful scenes demand more than three primaries that trades off the spatial resolution making it not suitable for architectural scenes with detailed patterns and facades. However, since current cameras come with a fixed number of primaries, users cannot change the spatial and spectral resolution as demanded by the scene conditions.

Main Contributions: We present a technique of *layering of a pair of color filter arrays (CFAs) with precise relative shifts* between them to achieve, for the first time, cameras with multiple operational modes where both the *number* and *transmittance* of the primaries can be changed. The user will thus have the liberty to cater the primaries towards specific scene conditions. Following are our main contributions.

1. We present the *first camera that can switch to three sets of color primaries on demand*. By using different relative shifts during the layering of the pair of CFAs, both the number and the transmittance of the primaries can be changed (Figure 2) to provide a camera with three different capture modes: RGB, CMY and RGBCY mode respectively (Section 2).

2. We extend the concept of shiftable layers of CFAs beyond switchable primaries showing that when applied to a different kind of CFA, it provides a *camera that can switch between low dynamic range (LDR) and high dynamic range (HDR)* modes (Section 3).

3. Next, we show that the general problem of finding the desired patterns and shifts of the CFAs to achieve predefined switchable operational modes can be posed as a *constraint satisfaction problem (CSP)*(Section 4). We show the utility of this general framework to design an add-on device for existing LDR color cameras that

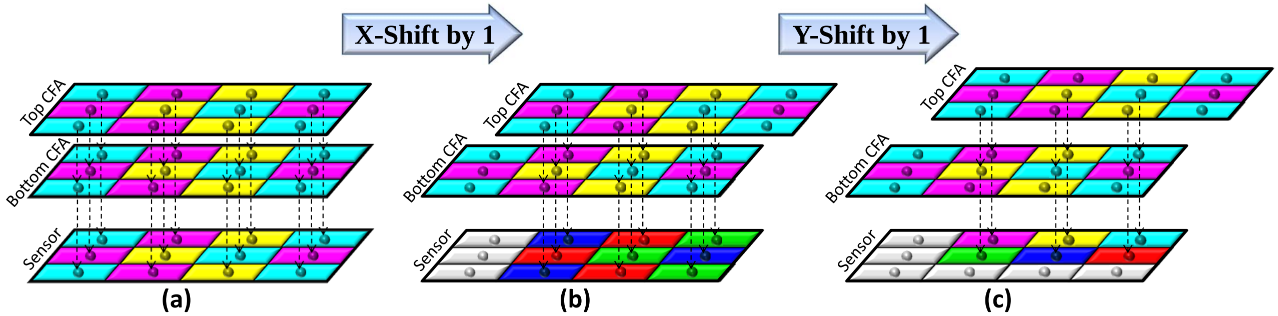

Figure 2: *Two CMY CFAs before shifting(a), after shifting the top layer one tile to the right(b), and after shifting the top layer by another tile in the vertical direction. The combinations of the layers, shown in the bottom, result in CMY(a), RGB(b), and RGBCMY(c) modes respectively.*

provide an additional HDR capability.
4. We present a quantitative cost-benefit analysis to show the benefits of a camera with switchable primaries: (a) when operated in the RGBCY mode, *significantly superior color fidelity* than traditional fixed RGB or CMY cameras is achieved (Section 5.1); and (b) the availability of both CMY and RGB color primaries in the same camera results in *optimal SNR, for both dark and bright scenes* (Section 5.2). Though layering CFAs marginally trades off the overall spectral transmittance of each primary, the benefits far overweigh this small shortcoming.
5. Finally, we propose several *practical design options* to embed such shiftable layers of CFAs in real cameras for multiple switchable operational modes (Section 6). We demonstrate the feasibility of such designs via rudimentary prototypes.

Related Work: Many different types of fixed CFAs have been invented and manufactured for photography [Lukac 2008], the most popular being the Bayer CFA [Bayer 1976]. [Yamagami et al. 1994; Gindele and Gallagher 2002; Susanu 2009; Hirakawa and Wolfe 2008; Kumar et al. 2009] use RGBW CFAs with white filter elements to sense more light than cameras with traditional Bayer CFAs. Fixed CFAs with more than three colors have been proposed to capture multispectral images [Shogenji et al. 2004; Baone and Qi 2006] sacrificing the spatial resolution for higher spectral resolution. These provide much higher color fidelity, but are still less accurate than an order of magnitude more expensive hyperspectral cameras. In contrast to all these works on fixed color primaries, our work is the first one that presents switchable color primaries by shiftable layers of CFAs.

On the other hand, our work supplements an earlier set of work on computational color in photography. Dynamic modification of spectral transmittance has been proposed in agile-spectrum imaging [Mohan et al. 2008] by using of diffraction grating. In a completely orthogonal domain, limited flexibility in color primaries has been explored via tunable sensors [Langfelder et al. 2009]. These sensors do not require CFAs to capture color images. Instead, each wavelength is captured at a different depth of the sensor. The absorbtion depth can be changed by applying an electrical voltage to the sensor. Therefore, the spectral-bands that are sensed at each depth can be tuned slightly. This allows for limited flexibility in the amount of overlap between the spectral response of the eye (CIE primaries for the standard observer) and that of the sensors, leading to a little higher color fidelity. However, this only allows a small shift in the spectral transmittance of the narrow band primaries, but cannot achieve a completely different number of primaries with entirely different spectral transmissivity as is possible in our camera.

2 Camera with Switchable Primaries

We achieve switchable color primaries by layering a pair of color filter arrays (CFAs) that can be shifted precisely relative to each other. For this we use a pair of CMY CFAs (Figure 2(a)), where each row repeats the C, M, and Y tiles. But odd rows start with C while even rows start with M. This results in the repetition of a 3×2 pattern of CMY tiles (Figure 2(a)).

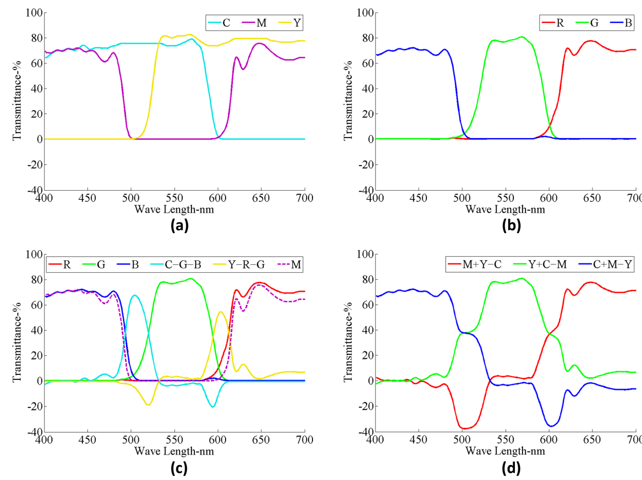

Figure 3: *Spectral transmittance of our primaries in (a)CMY mode, (b) RGB mode, and (c) RGBCY mode. In (c), the narrow band cyan and yellow are computed from the broad band CMY filters in (a) and the narrow band RGB filters in (b). (d) Spectral transmittance of the RGB channels demultiplexed from the CMY mode.*

When two such CMY CFAs are superimposed with no shift, tiles with similar spectral transmittance coincide and the combined effect is that of a CMY CFA, whose spectral transmittance is shown in 3(a). However, if the top layer is shifted by one tile horizontally, each C tile of the top layer superimposes a M tile of the bottom layer resulting in a B tile. Similarly, M and Y tiles of the top layer superimpose Y and C tiles on the bottom layer resulting in G and R tiles respectively. The spectral transmittance of these are shown in Figure 3(b). Therefore, with such a horizontal shift, this layered CFA is similar to an RGB CFA except for the first and last columns (Figure 2(b)). Finally, if the top layer is now shifted by another tile vertically (Figure 2(c)), in the odd numbered rows the C tiles superimpose Y tiles, and similarly M tiles superimpose C tiles and Y tiles superimpose M tiles, resulting in RGB tiles as before. But, in the even numbered rows the M tiles from the top layer superimpose with M tiles from the bottom layer, Y with Y and C with C resulting in broad-band CMY tiles (Figure 2(c)). Interestingly, we can compute narrow band cyan and yellow primaries, C_n and Y_n, where $C_n = C - B - G$ and $Y_n = Y - R - G$ (Figure 3(c)). But, since M is very close to $R + B$ (Figure 3(c)), we cannot similarly extract a sixth non-overlapping primary. This results in a capture mode with five almost non-overlapping primaries, namely R, G, B,

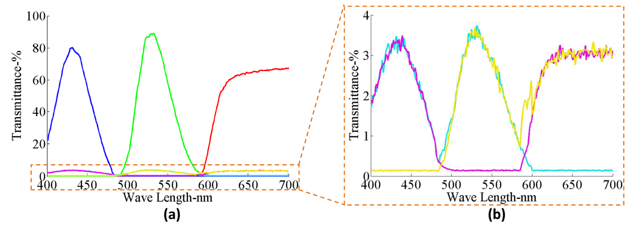

Figure 4: *(a) Spectral transmittance of the R, G, B, C_h, M_h, Y_h channels. (b) Zoomed-in view of the spectral transmittance of the C_h, M_h, and Y_h channels. The zoomed-in view shows that the RGB channels extracted from C_h, M_h, and Y_h are similar to the LDR RGB channels but are considerably less sensitive to light.*

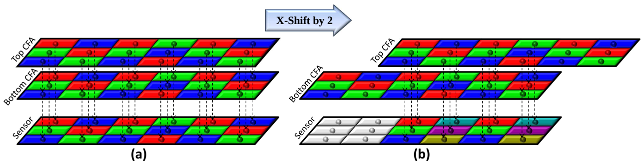

Figure 5: *Left: Two Layers of RGB CFA superimposed on each other. Right: The top layer is shifted 2 tiles to the right. After the shift the tiles that overlap with similar tiles work as RGB filters and the rest work as low transmittance CMY filters.*

C_n and Y_n, leading to a five primary mode – RGBCY. Thus, we achieve three different sets of color primaries in the same camera: (a) RGB, (b)CMY, and (c) RGBCY.

Our camera with switchable color primaries has several advantages over cameras with fixed RGB or CMY CFAs. Narrow band fixed RGB CFAs mimic the human eye, but do not have the desired light efficiency to provide a good signal-to-noise-ratio (SNR) for dark scenes. Wide band fixed CMY CFAs (Figure 3(a)), on the other hand, provide much better SNR for dark scenes. However, images need to be converted to the more common RGB format using demultiplexing computations of $R = M + Y - C$, $G = Y + C - M$ and $B = C + M - Y$. These computations introduce greater noise for bright scenes. Further, the effective spectral transmittance profiles of the R, G, B channels following this computation (Figure 3(d)) can be negative leading to lower color fidelity due to clamping artifacts [Cao and Kot 2008]. Thus, while CMY cameras are better for dark scenes, RGB cameras are preferred for bright scenes. In summary, our camera can provide optimal SNR by capturing dark scenes in the CMY mode and bright scenes in the RGB mode; and can also provide significantly higher color fidelity for colorful scenes in the RGBCY mode.

We have demonstrated and evaluated the superior color fidelity and optimal SNR achieved by our camera using empirical results (Section 5) obtained from multiple prototypes designed and built in our lab (Section 6).

3 Camera with Switchable Dynamic Range

The same concept of shiftable layers of CFAs can be used to create different operational modes, beyond just switchable primaries. When creating switchable primaries, we considered layers of CMY CFAs. Now, let us consider RGB filters that have a small transmittance over the entire spectrum (Figure 4a) in addition to the peaks in the R, G, and B regions respectively. In this scenario, superimposition of unlike filters – i.e. B and G, R and B, or R and G – result in very low transmittance cyan, magenta and yellow filters, C_h, M_h and Y_h, respectively.

Let us now consider two layers of RGB CFAs (Figure 5). Before shifting, similar tiles superimpose (Figure 5a) resulting in a low dynamic range (LDR) capture mode. But, with a relative horizontal shift of 2 tiles (Figure 5b) we get a column of RGB filters and another column of CMY filters with very low transmittance that are sensitive to a higher range of brightness. Hence, in this mode, we can capture high dynamic range (HDR) image while marginally trading off the spatial resolution. Thus, we now get a camera which can switch between LDR and HDR capture modes. We describe prototypes for such a camera and results thereof in Section 6 and 5.

4 A General Framework

In general, we can pose the problem of designing appropriate CFA patterns and their relative shifts as a *constraint satisfaction problem (CSP)*. We impose constraints on the combinations of the primaries and their proportions in each capture mode which are then solved by a CSP solver to return the patterns for both the CFAs.

Let us assume p different tiles/filters, $F_k, 1 \leq k \leq p$. For example, in the context of Figure 2, there are 6 different tiles, (C,M,Y,R,G,B). First, we define the set of valid combinations of the tiles that can be used in the design. This is a set, V, of 3-tuples that define the tile in the top layer, bottom layer, and their combination. For figure 2, $V = \{(M,Y,R),(Y,C,G),(C,M,B),(C,C,C),(M,M,M),(Y,Y,Y)\}$. In all the examples in this paper, switching the first two elements of the 3-tuple also result in valid combinations, but we omit those 3-tuples for compact representation. Next, for each capture mode, we define the desired proportion of each primary in the final combination. We assume m capture modes. For each mode $l, 1 \leq l \leq m$, we define as a p-tuple, M_l, which specifies the proportions of tile F_k in mode l. For Figure 2, $M_1 = (\frac{1}{3},\frac{1}{3},\frac{1}{3},0,0,0)$, and defines the CMY mode; $M_2 = (0,0,0,\frac{1}{3},\frac{1}{3},\frac{1}{3})$ and defines the RGB mode; and finally $M_3 = (\frac{1}{6},\frac{1}{6},\frac{1}{6},\frac{1}{6},\frac{1}{6},\frac{1}{6})$ and defines the RGBCMY mode.

In order to find the CFA patterns, the CSP solver starts the search from the smallest possible number of tiles that can fit all the desired proportions defined by M_ls. Among different sizes with the same number of tiles, it starts the search from the one which is closest to a square in shape. Lets assume the size of the pattern is (n_x, n_y). Lets define the tiles of the top and bottom layers as $T(i, j)$, and $B(i, j)$ respectively, where $0 \leq i < n_x, 0 \leq j < n_y$. The combination of the layers, however, depends on the additional parameters of the direction and magnitude of the relative shift between the two layers. Therefore the solver also iterates on the possible shifts starting from the smallest one. Let us assume for mode l the shift is defined by (x_l, y_l) and the superposition of the two layers as $S_l(i, j)$. Consequently, we enforce the following combination constraints:

$$(T((i+x_l) \bmod n_x, (j+y_l) \bmod n_y), B(i,j), S_l(i,j)) \in V \quad (1)$$

Further, we also impose proportion constraints for each filter F_k assuring that its total number in the combined layer for mode l confirms to M_l. This constraint is as follows.

$$\sum_{ij}(S_l(i,j) == F_k) = M_l(k) n_x n_y \quad (2)$$

Since each of the above constraints only affects a few variables, they can be efficiently solved by standard CSP solvers. In addition to these, we can also impose constraints on the amount and direction of the shift. For example, for a switchable CMY/RGB/RGBCMY camera, if we impose an additional constraint to limit the shift only in the horizontal direction, the CSP solver fails to find a pattern with only 6 tiles. However, after increasing the size of the pattern, it finds the 4×3 pattern in Figure 6 where the CMY, RGB and RGBCY modes are achieved by 0, 1 and 2 tiles horizontal shift respectively.

Further, we can impose constraints on one of the layers to have a specific pattern. For example, if we desire to build a switchable

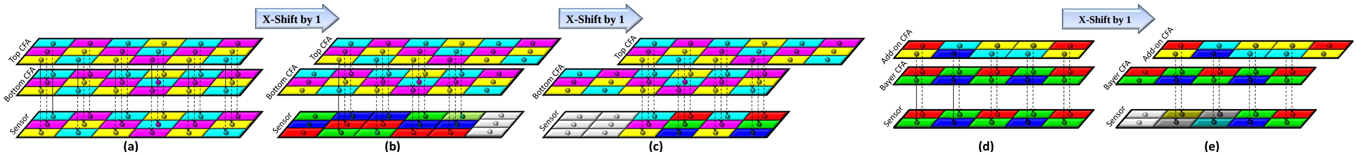

Figure 6: *Results returned by CSP solver. (a),(b), and (c): Layering of two CMY color filters to create a camera with switchable primaries with the shift constrained to be in only one direction – CMY mode before shifting (a), RGB mode after shifting one of the layers one tile to the right (b), and RGBCMY mode after shifting 2 tiles to the right. (d) and (e): Layering of a add-on CFA by constraining one layer to be a Bayer CFA to create a camera with switchable LDR and HDR modes – the add-on pattern does not considerably affect the transmittance when superimposed with a Bayer CFA without shifting giving the LDR mode (d), when shifted to the right on a Bayer CFA, some of the tiles are similar to RGB filters and the rest become low transmittance ICY filters which capture HDR values providing the HDR mode (e). Note that unlike all other CFAs in the paper, this has C, Y, R and B filters – not just CMY or RGB filters.*

LDR/HDR camera using a commodity camera with an existing Bayer CFA on the sensor, we can specify $B(i,j)$ to form a Bayer pattern and let the solver find only $T(i,j)$. In this case, we have 6 tiles (R,G,B,C_h,M_h,Y_h) and the valid combinations are $V = \{(R,R,R),(G,G,G),(B,B,B),(G,B,C_h),(B,R,M_h),(R,G,Y_d)\}$. There are two capture modes – LDR and HDR. In the LDR mode, the Bayer pattern dictates $M_1 = (\frac{1}{4},\frac{1}{2},\frac{1}{4},0,0,0)$. However, note that it is difficult to define specific proportions for the low transmittance tiles of C_h, M_h and Y_h since multiple different combinations may all produce acceptable results. In such scenarios, we can define a range of proportions instead of a specific one. For example, we can define $M_2 = (\frac{1}{8},\frac{1}{4},\frac{1}{8},[\frac{1}{8}\frac{1}{4}],[\frac{1}{8}\frac{1}{4}],[\frac{1}{8}\frac{1}{4}])$. Finally, one can also impose constraints on the patterns themselves to enforce certain desired properties such as non-adjacency of similar filters, or equal number of other filters in the neighborhood of each filter.

However, note that a CSP solver may not always return a solution. For example, this is the case for the above set of constraints defined for the switchable LDR/HDR camera. One way to alleviate the situation in such scenarios is to provide more sets of valid combinations. For example, we can add constraints to denote that R, G and B can be generated differently than just superimposing two layers of R, G and B. This can be achieved by adding $\{(Y,R,R),(C,G,G),(M,B,B)\}$ to the aforementioned V . Further, we can also experiment with different filters. For example, instead of having C_h, M_h and Y_h as the low transmittance filters, we can have an equivalent set of C_h, I_h, and Y_h where I_h is an intensity filter and replaces M_h. Thus, in this case, we have a set of six different filters (R,G,B,C_h,I_h,Y_h) where the valid superpositions for achieving I_h are given by $\{(C,R,I_h),(M,G,I_h),(Y,B,I_h)\}$. By doing these changes, the CSP solver can now provide a solution for an add-on CFA to the Bayer CFA to achieve switchable LDR and HDR modes, as shown in Figure 6. Note that the top layer here consists of C, Y, R and B tiles, instead of having just *CMY* or *RGB* tiles. We build a sample prototype for this, as explained in Section 6. However, note that in the LDR mode, R can be formed both by superimposing two R tiles or a R and a Y. Similarly, G and B can also be generated in two ways resulting in varying spectral transmittance of the same primary in this mode. However, we find in our prototype that this still produces acceptable results (Figure 14).

Another way to assure a solution from the CSP solver is to weigh some constraints to be more important than the others. For example uni-directional shift can be an important design constraint, while non-adjacency of similar filter may not be as critical. Allowing such weights in the CSP solver results in a Markov Random Field that can be solved efficiently using AI techniques for bounded search.

5 Results

For the proof of concept of our camera with switchable operational modes, we used a time sequential capture of images using different layers of color filters in front of a monochrome camera to simulate the shiftable layers of CFAs (Figure 7). For demonstrating switchable primaries, we captured the images by superimposing pairs of CMY filters, both like (C and C, M and M, and Y and Y) and unlike (C and M, M and Y, and C and Y). For demonstrating switchable LDR/HDR mode, we captured images by superimposing RGB filters. Next, to simulate the effect of capturing all these in a single shot, we pick each pixel from the appropriate image in this temporally multiplexed sequence. The image thus created, records only one primary at every pixel simulating the effect of the layered CFAs. We demosaic these image in software (Section 7) to achieve the final full-resolution image for either CMY, RGB or RGBCY modes. The setup of Figure 7 provides us with high quality and high resolution results to prove the concept of shiftable layers of CFAs. However, alternate practical designs for such a camera without time multiplexing is described in Section 6.

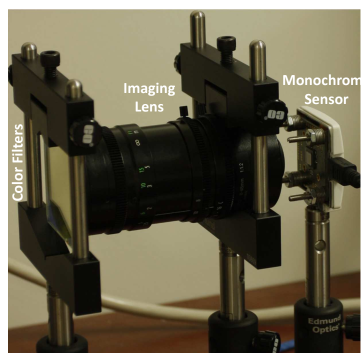

Figure 7: *Our first prototype where color filters are temporally multiplexed to simulate our camera.*

For the setup in Figure 7, we used a monochrome 2560×1920 camera (EO-5012BL [2]) and dichroic filters from *EdmundOptics* [1]. The spectral transmittance of the CMY filters (Figure 3) are obtained from the specifications in the manufacturers website [1]. For the LDR/HDR camera, we create RGB color filters by exposing 35mm Kodak films to appropriate lighting. To allow some amount of light (at least 4%) to pass through in the HDR mode after the superposition of the shifted layers, we did not fully expose the films. Figure 4 shows the transmittance profiles of these filters captured using a SOC-730 hyperspectral camera.

Figure 8 shows the results for the switchable LDR and HDR modes. We use an adaptive logarithmic tone mapping operator [Drago et al. 2003] to show the HDR image. Figures 9, 10 and 11 show the results for the camera with switchable primaries. In the rest of the section, we quantify the advantage of our camera with switchable primaries.

5.1 Superior Color Fidelity

First, we discuss the superior color fidelity of our camera with switchable primaries in the RGBCY mode when compared to the RGB or CMY modes. For this we compared the images captured by each mode of our prototype camera against those cap-

[2] http://www.edmundoptics.com/onlinecatalog/displayproduct.cfm?productID=1734

[1] The transmittance profile is available at http://www.edmundoptics.com/onlinecatalog/displayproduct.cfm? productID=2947

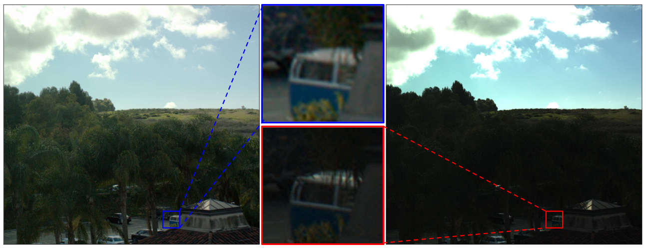

Figure 8: *Left: A scene captured with the HDR mode of our camera with switchable LDR and HDR mode . Right: The same scene captured with the LDR mode of our camera (saturated sky and dark trees). On the other hand, in the zoomed-in view the resolution of the LDR image is higher than the HDR one, emphasizing the need for flexibility based on the scene and application.*

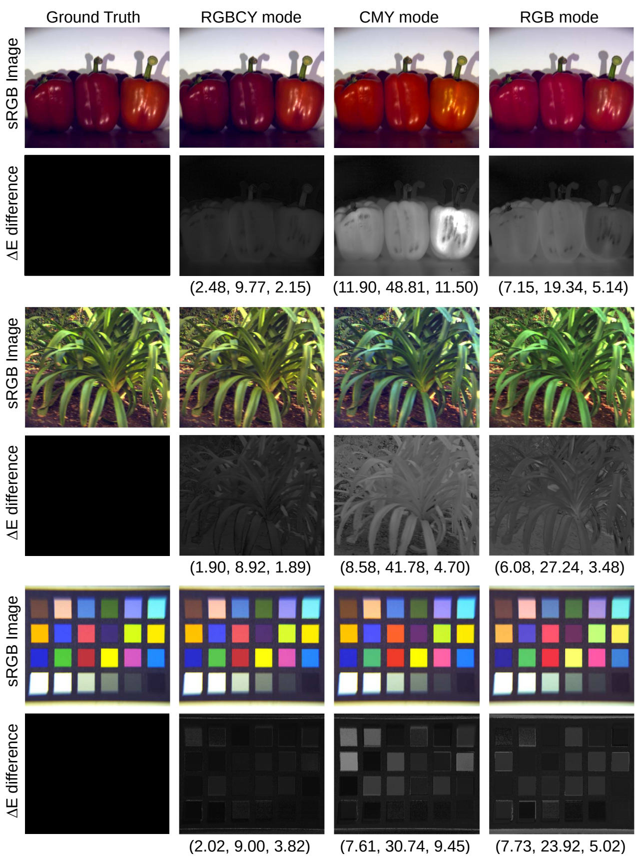

Figure 9: *Three examples of comparison between the ground truth images captured with a* SOC-730 *hyperspectral camera and images captured with our prototype camera with RGB, CMY, and RGBCY capture modes. The gray images show the CIELAB* ΔE *difference from the ground truth for each image along with the error statistics (mean, maximum and standard deviation from mean). Note the better color fidelity of the RGBCY mode, especially in the red-purple and cyan-green colors. Also, note that in general the color fidelity of CMY mode is much lower than the RGB mode.*

tured by a *SOC-730* hyperspectral camera at a spatial resolution of 1024×1024 and spectral resolution of around $9nm$ in the range of visible wavelengths from $420nm$ to $700nm$. We used a data set of 35 such images.

For comaparison, we generate four images in the CIE XYZ space. First, we compute a ground truth image from the captured hyper-

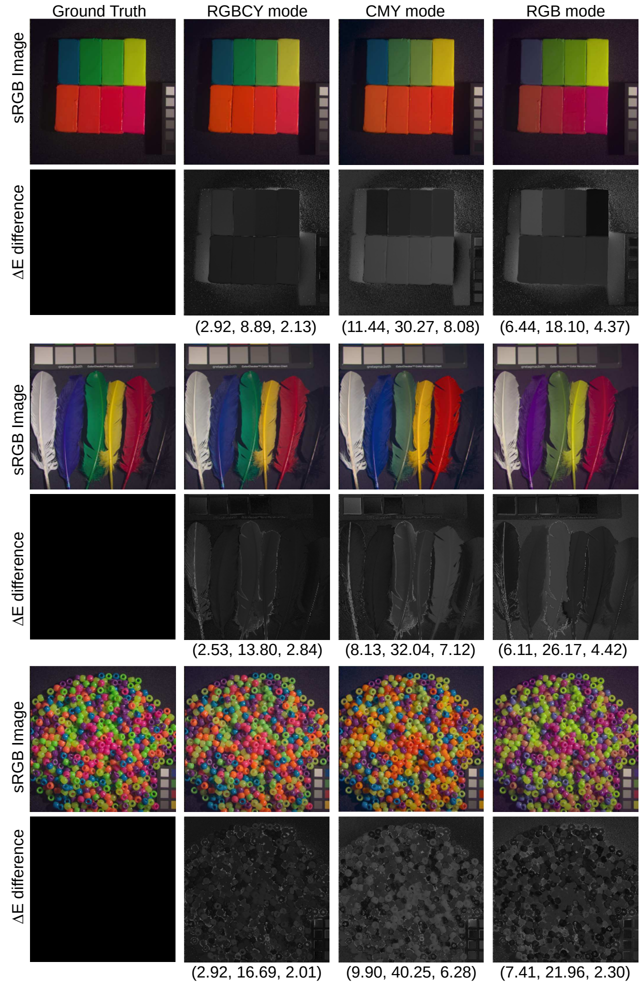

Figure 10: *Three examples of comparison between the ground truth and simulated images for RGB, CMY, and RGBCY capture modes using the CAVE multi-spectral database. The gray images show the CIELAB* ΔE *difference from the ground truth for each image along with the error statistics (mean, maximum and standard deviation from mean). Note the superior color fidelity of the RGBCY mode when handling near-saturated shades of blue, green, and red.*

spectral image by finding the CIE XYZ values at each pixel via a scalar dot product of the spectral response at that pixel, $P(\lambda)$, with the the standard observer's sensitivity for the three sensors in the eye, $x(\lambda)$, $y(\lambda)$ and $z(\lambda)$ respectively. Next, we convert the images captured by the three different modes of our prototype to CIE XYZ space. The XYZ value corresponding to the captured color is computed by a weighted sum of the captured values, where the weights for each of the X, Y and Z are computed by finding the correlation of the known spectral transmittance profiles of the primaries (Figure 3) with $x(\lambda)$, $y(\lambda)$ and $z(\lambda)$ respectively. To quantify the perceptual difference of each of these camera captured images from the ground truth, we compute their ΔE differences in the CIELAB space. Further, to provide a feel of how these images would look on a standard sRGB display, we convert them to the sRGB space. Since the ΔE images do not involve errors due to clamping, they are better indicators of the differences seen by a human. To align the images captured by our camera and those from the hyperspectral camera, we use standard rectification techniques.

Figure 9 shows a few examples from this set of 35 images along with the statistics (mean, maximum, and standard deviation from

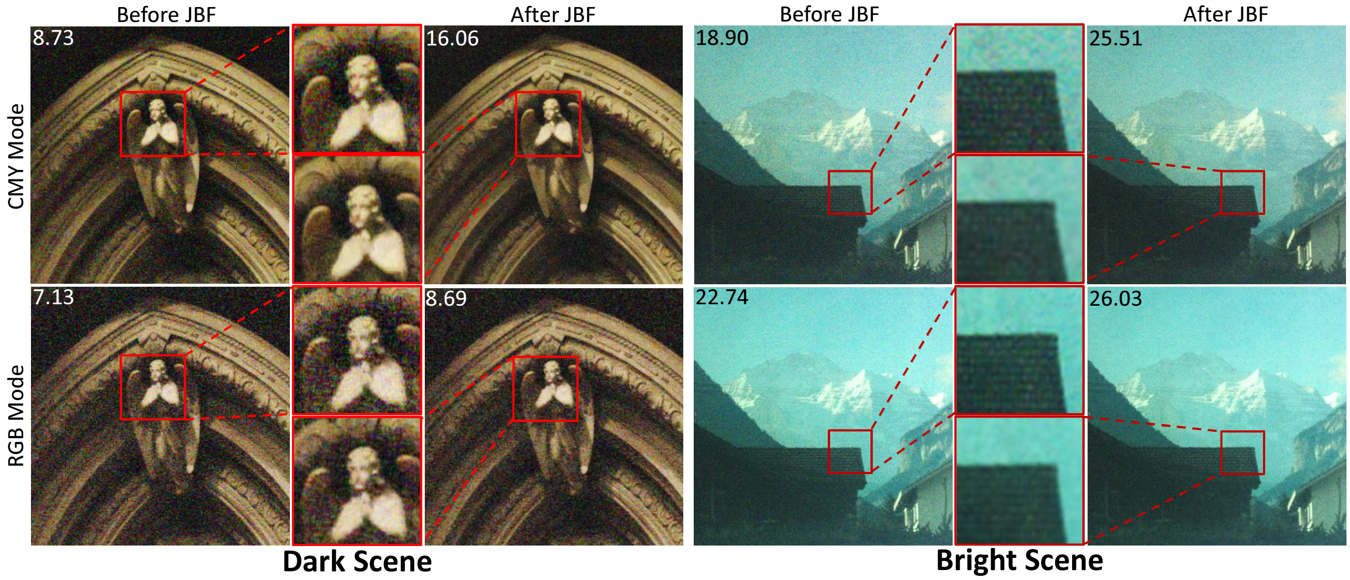

Figure 11: *Scenes captured with CMY (top) and RGB (bottom) modes of our camera is shown before (left) and after (right) applying the JBF for a dark and a bright scene. The SNR are embedded on the top right of each image. For the dark scene, the CMY mode provides superior SNR, particularly after applying the JBF. For the bright scene, the RGB mode provides superior SNR. The JBF reduces the noise but degrades the overall perceptual quality of the image because of the reduced sharpness of the edges.*

the mean) of the per-pixel ΔE error for each of these images. The average ΔE difference, over all the 35 images, for RGBCY mode was 1.95 units and 6.2 and 7.5 units for the RGB and CMY modes respectively. This is a perceptible difference of more than 1JND (3 units of ΔE = 1 JND). Further, note that the RGBCY mode reduces the maximum deviation from the ground truth tremendously, when compared to the RGB and CMY modes – but some deviation still remains since five primaries are not sufficient to achieve the color fidelity of a hyperspectral camera with 30 spectral bands.

In order to confirm the same result for an existing standard database, we use the CAVE multi-spectral image database [Yasuma et al. 2008] that includes 31 pictures sampling the range of the visible wavelengths from 400*nm* to 700*nm* at 10*nm* increments at each pixel. We simulate the images captured by the camera in different modes using the spectral transmittance profile of the primaries (Figure 3) of that mode. Then, we compute the same ΔE difference as mentioned above for the simulated camera images in different modes.

Figure 10 shows a few examples along with the statistics (mean, maximum, and standard deviation from the mean) of ΔE error. The results are similar to the first set of experiments with an average ΔE difference of 2.12, 6.5 and 7.6 units for the RGBCY, RGB and CMY modes respectively. This confirms a significantly improved color fidelity in the RGBCY mode.

5.2 Optimal Signal to Noise Ratio

The signal-to-noise-ratio (SNR) of an image is strongly related to the spectral properties of the color filters and the overall brightness of the scene. CMY CFAs are known to have higher SNR compared to RGB CFAs in dark scenes due to their higher spectral transmittance; but result in lower SNR for brighter scenes since the noise adds up when demultiplexing the RGB values from the captured CMY values. Our camera offers the best of both worlds by switching between RGB and CMY modes.

To demonstrate this, we present in the appendix a computational method to analyze the SNR of our camera theoretically. We compute two ratios, $\frac{SNR_{CMY}}{SNR_{RGB}}$ and $\frac{SNR_{CMY}}{SNR_{RGBCY}}$ (Equation 3), for both bright and dark scenes (Table 1). These are computed for captured color vectors C and for the intensity value g, obtained by the sum of the captured values across the multiple channels.

	$\frac{SNR_{CMY}(C)}{SNR_{RGB}(C)}$		$\frac{SNR_{CMY}(C)}{SNR_{RGBCY}(C)}$		$\frac{SNR_{CMY}(g)}{SNR_{RGB}(g)}$		$\frac{SNR_{CMY}(g)}{SNR_{RGBCY}(g)}$	
	M	P	M	P	M	P	M	P
Dark	1.25	1.22	1.94	1.99	2.08	2.12	0.94	0.96
Bright	0.85	0.84	1.60	1.57	1.39	1.37	0.82	0.82

Table 1: *Comparison of SNR ratios for C and g across CMY, RGB, and RGBCY capture modes. M denotes measured and P denotes predicted. Note that for all conditions, the measured ratios conform closely to the predicted ones validating our SNR model.*

To validate the model in practice, we measure the same ratios for a set of images captured by our prototype (Section 6) and compare them with those predicted using our SNR model in Equation 3. We use images of 20 different scenes for each of the dark and bright conditions, and we capture the same scene 25 times under the same illumination for each mode. To achieve such a controlled illumination for this experiment, we use projector based illumination over a printed scene to vary the scene conditions from dark to bright. We vary the exposure time inversely proportional to the illumination intensity.

To find the SNR for each scene, we first find the mean and variance estimators of the captured color vectors at each pixel using the 25 images captured under the same illumination. From this, we can compute the per pixel noise-to-signal ratio which are then averaged across the pixels and inverted to find the average SNR of C. To find the SNR of g, we repeat the same process, but instead of using the color vectors, we use the sum of all the captured values.

Table 1 shows the predicted and measured SNR ratios for both C and g. The closeness of the predicted and measured values in this table validates the accuracy of our noise model and show that for dark scenes, the SNR is more than 20% higher in the CMY mode than the RGB mode. But, for bright scenes, the RGB capture mode shows similar SNR advantage over the CMY mode. Also, when compared to the RGBCY mode, the CMY mode has almost double the SNR for dark scenes. This is due to the very narrow band C_n and Y_n primaries in the RGBCY mode. Thus, the greater color fidelity of the 5 color mode comes at the cost of reduced SNR.

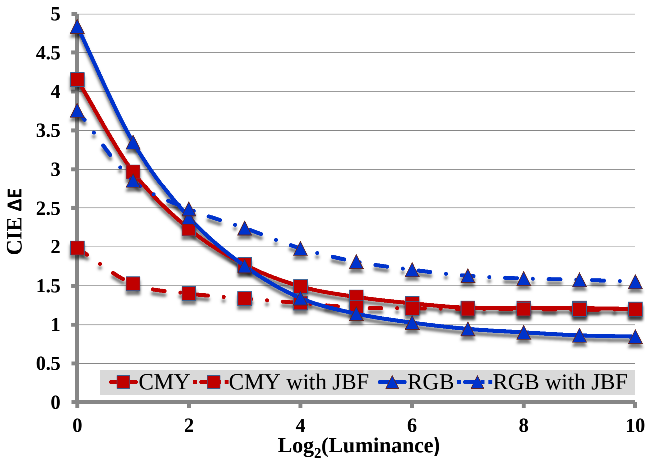

Figure 12: Δ*E difference from ground truth increasing luminance level for RGB and CMY modes before and after the JBF. Longer exposure time is used for lower luminance levels such that the amount of light that reaches the sensor remains constant. The longest exposure is 2 seconds and the shortest is 1 millisecond. We used ISO 400 for this experiment. The graph demonstrates that for low luminance levels CMY capture mode is superior particularly after applying the JBF. On the other hand, for high luminance levels RGB capture mode without JBF results in superior SNR while the JBF degrades the quality of the image.*

Joint Bilateral Filtering: Table 1 shows that the SNR for g is much superior than the SNR for C, especially in the CMY mode (almost 2 times), for both dark and bright scenes. Hence, we propose using the intensity image g, obtained by adding all the primaries, as a guidance image to apply joint bilateral filtering (JBF) on each channel of the captured image to achieve better SNR. However, JBF can also degrade the image fidelity by blurring the high-frequency details. Hence, there is a trade off involved in the improvement in the SNR and the degradation in image fidelity.

To evaluate this, we find the SNR of a scene after applying JBF for a particular mode using the aforementioned SNR analysis using the same set of 20 scenes after applying JBF. From this we find that for *dark scenes*, JBF improves the SNR of the CMY mode dramatically but does not affect the SNR of the RGB mode as much. Hence, after JBF, the CMY mode provides almost 70% better SNR than RGB mode (as opposed to 20% improvement without JBF).

For *bright scenes* also, JBF improves the SNR. But this comes at the cost of degradation of the image fidelity. We measure this degradation using ΔE difference of the captured image, before and after applying the JBF, from a ground truth image in both CMY and RGB mode. To find the ground truth for each scene in a particular mode, we average the 25 images captured under the same illumination. Finally, we average these values thus computed across all the pixels and all the scenes captured in this mode to find the ΔE difference of it. From this metric, we find that the degradation in the image fidelity due to the JBF, offsets the improvement in the SNR in RGB mode much more than in CMY mode (Figure 12). Hence, for bright scenes, the highest image fidelity is achieved in the RGB mode without applying the JBF.

6 Design Options and Prototypes

In this section, we provide design options for embedding shiftable layers of CFAs in a real camera. We build some prototypes based on these designs and show some preliminary results from them.

6.1 Mechanical Shift

The easiest way to achieve shitable layers of CFA is to layer two CFAs on the CCD sensor during manufacturing. However, one of them should be equipped with a shift mechanism. This can be achieved using inexpensive (less than $175) linear staging devices devices (e.g. EdmundOptics Part Number NT56-416 [5])) some of which allow linear shifts with 1 μm accuracy.

To demonstrate the feasibility of this design, we used it to build a rudimentary prototype of our camera with switchable primaries. We opened up a monochrome 2560×1920 camera (*EO-5012BL from EdmundOptics*) to expose its CCD sensor. We used printed 35mm digital slides for the CFAs. Such slides can be printed in professional photo labs such as Swan Photo Labs [3] and cost about $4 for each slide. To implement the shift of one of the CFAs, we used a Metric Bar-Type Lens Holder [4] (price: $79). One of the CFA layers is mounted on the static part of the holder and the other one is mounted on the moving part (Figure 13). The screw on the moving section has 20 teeth each of height 0.5mm. Therefore, one turn of this screw results in 0.5mm shift of the moving CFA. Hence, by rotating the head of the screw by one degree in each direction we can move the part about 1.39μm.

However, this setup has a tremendous scope of improvement when used for production. Our cheap CFAs has neither the resolution nor the light efficacy of the much superior glass CFAs used in standard cameras. The minimum size of the pixels in our printed patterns is $8.8\mu m \times 8.8\mu m$ resulting in 4 times bigger pixel size in each dimension than our monochrome camera pixels ($2.2\mu m \times 2.2\mu m$). Further, the pixels are printed using light beams which do not produce rectangular pixels but gaussian blurs. Therefore, we printed a pattern with 2 times larger pixels and one black line between every two adjacent pixels to prevent color bleeding. Consequently, a CFA pixel becomes 12 times bigger in each dimension when compared to a sensor pixel. To alleviate this mismatch in the pixel size, we separate the CFAs from the sensor. The image is first focussed on the CFAs and refocused on the sensor using an achromatic lens (25mm diameter and 30mm effective focal length). This lens also downsizes the CFA pixels by a factor of 3 in each dimension making the resolution mismatch a factor of 4 in each dimension. Even when considering the 4×4 pixels on the sensor which are considered as one pixel of the prototype, we observe considerable color bleeding between the adjacent pixels resulting in blurry CFA tiles. This is due to the glass cover over the sensor which acts as a diffuser. We could not remove this glass cover due to the fragility of the sensor. Hence, to nullify its effect we only consider the 2×2 center pixels of this 4×4 groups of pixels in the sensor and average their values to get the captured values. All these result in an overall large degradation in image quality and a low-resolution image of 640×480. Figure 13 shows the picture of this prototype and some images captured by it. Further, in terms of size, note that 16cm length of our 19cm long prototype contributes to refocus the image from the CFA to the imaging sensor which is unnecessary when one layer of the CFA is mounted directly on the sensor. Finally, in terms of cost, the off-the-shelf devices that are used in our setup are not custom tailored for our application (for e.g. the Metric

[5] http://www.edmundoptics.com/onlinecatalog/displayproduct.cfm?productID=1844

[3] http://www.swanphotolabs.com/swan08/

[4] http://www.edmundoptics.com/onlinecatalog/displayproduct.cfm?productID=2190/

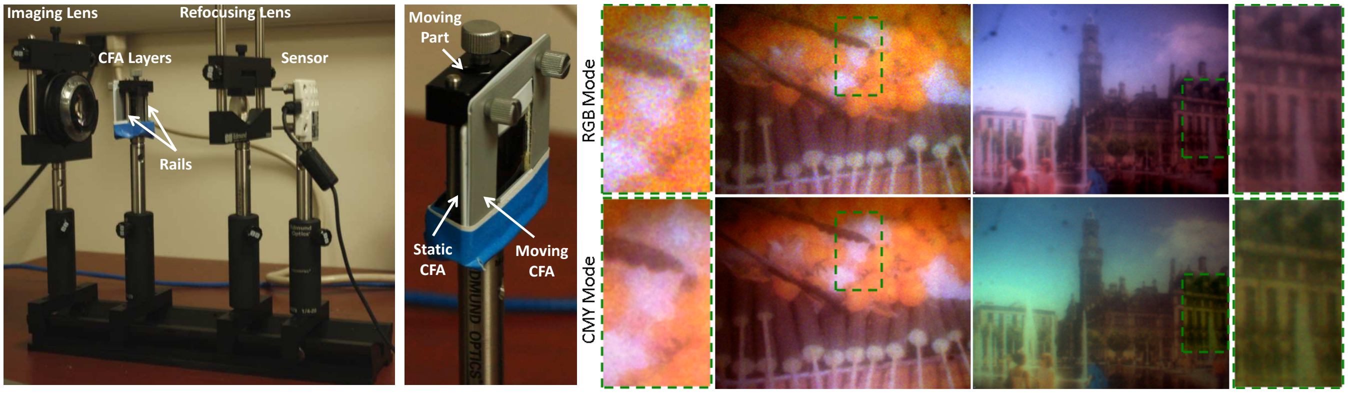

Figure 13: *Left: Picture taken from our sample preliminary prototype. Middle: Zoomed-in view of the shifting mechanism from a different angle. Right: Images taken with our prototype with RGB and CMY modes in different lighting conditions. Please note the better SNR of the CMY mode for the dark scene (left) and the better SNR of the RGB mode for the lighted scene (right) in the zoomed-in views.*

Figure 14: *Left: This figure shows the design of the add-on device that be added to a regular Bayer LDR camera to achieve a HDR mode. A pair of lens, separated by a fixed distance, is put between the Bayer CFA on the camera sensor and the printed CFA. The lens which is close to the CFA is slightly off-axis. The amount of shift is controlled moving this two-lens ensemble on a rail. Right: We show the LDR and HDR images captured by this prototype. Note the saturated sky in the LDR mode is better captured in the HDR mode.*

Bar-Type Holder can hold much heavier weight than is required by a camera). Devices designed specifically and mass produced for a camera can turn out to be considerably cheaper.

6.2 Optical Shift

We also investigate another design which can be used as an add-on device on a DSLR camera to make it a camera with switchable modes. In this setup, the image is formed on the first CFA layer and then refocused on the second CFA layer which is attached to the sensor. The refocusing is done using two convex lenses with the same power. However, by making one of these lenses slightly off-axis we can shift the image in the off-axis direction. A precise shift can be obtained by controlling the placement of the lenses between the first CFA and the sensor (Figure 14).

Let us assume the first lens is α units off-axis and the desired shift is β units. The magnification of the two lenses are s_1 and s_2 respectively, where $s_1 s_2 = 1$. Assuming the second lens is axis aligned, the total shifting of the image is $s_2\alpha = \frac{\alpha}{s_1}$. We desire this shift to be β. Hence, $s_1 = \frac{\alpha}{\beta}$. Using standard thin lens equation, we find that in order to achieve this scale factor the first lens should be placed at distance $d_1 = \frac{f(s_1+1)}{s_1}$ from the CFA. The resulting image will be at distance $\frac{f(s_1+1)^2}{s_1}$ from the CFA. In order to make $s_2 = \frac{1}{s_1}$, using thin lens equation, we find that the second lens should be at a distance $f(s_1-1)$ behind the image of the first lens. Therefore the second lens should be placed at $d_2 = \frac{f(s_1+1)^2}{s_1} - f(s_1-1) = 2f + x_1$ and the image of this lens will be formed at $x_2 + \frac{f(s_1-1)}{s_1} = 4f$. Thus, irrespective of s_1 and s_2 the distance between the CFA and the sensor should be $4f$ and the distance between the lenses should be $2f$. Different β can be achieved just by moving the lens pair to different positions between the CFA and sensor.

The main advantage of this setup is that a small movement of the CFAs can be precisely controlled by a few orders of magnitude larger movement of the pair of lenses. For example in our setup we used two lenses with $f = 3cm$. When we do not want to shift the image, we can simply place the first lens at distance f from the first CFA. In the shifted state, we chose $\alpha = 10\beta = 264\mu m$. Therefore, $x_1 = \frac{f(s+1)}{s} = 3.3cm$. Thus, we can achieve $26.4\mu m$ shift by moving the lenses $3mm$ away from the CFA. Further the setup can be considered as an addition to any normal camera with wide-band CFA without changing any of the parts inside the camera. However, in terms of size, this is relatively large since the image is focused twice on the two CFA layers.

We used this optical shift to design a prototype switchable LDR/HDR camera. We use a Canon Rebel Xsi camera which has a Bayer CFA on its sensor. Then we use the CFA presented in Figure 6 for the second CFA layer. Finally, we used two lenses with $25mm$ diameter and $30mm$ effective focal length with the first lens moved $264\mu m$ off-axis to achieve the optical shift. For CFA, we used 35mm digital slides. All the issues of resolution and quality degradation that exists in the previous prototype also exists here and are handled similarly. However, since at least one layer of the CFA is a high quality one, we achieve better results (Figure 14).

7 Discussion

Demosaicing: Our camera with switchable modes have novel CFA patterns whose behavior to standard demosaicing is studied here. There are several demosaicing methods in the literature, often suitable for particular CFA patterns. Freeman [Freeman 1988] uses a median filter to process the inter-channel differences of demosaiced images obtained by bilinear interpolation. Some other methods investigate the spatial and frequency characteristics of the image to achieve better demosaicing. For example, edge classifiers are often used to identify the best directions for interpolating the missing color values [Li 2005; Hamilton and Adams 1997]. [Gunturk et al. 2002] uses a scheme to exploit spectral correlation by alternately projecting the estimates of the missing color values onto constraint sets based on original CFA samples and prior knowledge of spectral correlation.

	Bilnear	Gunturk	Li	Lu & Tan	**Minimum**
Switch/Fig 1					
RGB	1.07	1.03	1.01	**0.92**	**0.92**
CMY	1.11	0.98	**0.92**	1.00	**0.92**
RGBCY	1.40	1.28	1.18	**1.16**	**1.16**
Switch/Fig 11					
RGB	0.80	0.78	0.76	**0.71**	**0.71**
CMY	1.08	0.98	0.89	**0.88**	**0.88**
RGBCY	1.39	1.28	1.17	**1.16**	**1.16**
LDR/HDR					
LDR	0.84	0.83	0.75	**0.70**	**0.70**
HDR	1.63	1.48	**1.39**	1.41	**1.39**
Bayer	0.82	0.79	0.74	**0.73**	**0.73**

Table 2: *Comparison of the performance of several demosaicing methods for different capture modes of our camera. We used CIELab difference from a non-mosaics image as the error metric.*

In addtion to bilinear interpolation, we experimented with several more recent demosaicing methods [Gunturk et al. 2002; Li 2005; Lu and Tan 2003] to evaluate their suitability for our particular CFA patterns in Figures 2, and 6. To quantify this, we find the average ΔE difference of the demosaiced image from the original non-mosaiced image in the CIELAB space. We also compare this to the error due to demosaicing for a Bayer pattern.

Table 2 summarizes this evaluation and shows that though most methods work well for the different modes, each mode favors some demosaicing methods over others. Most importantly, demosaicing artifacts from the RGB mode of the pattern in Figure 2 is comparable to the Bayer pattern and even slightly better when considering the minimum error of the methods. However, the pattern in Figure 6 shows higher error in the same mode primarily due to adjacent tiling of similarly colored filters. Also, the CMY mode of both our patterns show more error than the RGB mode. Finally, the RGBCY mode shows more error than RGB or CMY mode. This emphasizes the need for camera with switchable primaries where lesser noise and demosaicing artifacts can be traded over color fidelity when it is not of critical importance. Further, like any single shot HDR camera, our camera with switchable LDR and HDR mode compromises spatial resolution in HDR mode (Figure 8). This manifests itself as larger demosaicing errors for the HDR mode than the LDR mode.

Effects on Light Efficiency: Usually RGB CFAs are built using layered combinations of CMY dyes [Gunturk et al. 2005] in a fashion equivalent to our RGB mode. Hence, layering CFAs does not compromise the spectral transmittance in the RGB mode of the switchable camera. Since the current filters have light efficiency close to 90%, even in the CMY mode, there is only a small loss in the light efficiency (around 10%) that is outweighed by the 70% improvement in the SNR in this mode.

8 Conclusion

In summary, we present the concept of shiftable layering of CFAs to achieve multiple switchable operational modes within the same camera. We demonstrate two different cameras using this concept: a camera with switchable primaries that can operate in the RGB, CMY and 5-color RGBCY modes; and a camera with switchable LDR and HDR capture modes. The camera with switchable primaries can provide superior color fidelity for colorful scenes and the optimal SNR for both dark and bright scenes. The camera with LDR and HDR modes can trade off resolution to capture a higher dynamic range. Further, we show that the general idea of CFA layering can be posed as a constraint satisfaction problem to find CFA patterns based on the design constraints. Finally, we propose some simple designs to explore the practical feasibility of embedding such shifted layering of CFAs in real cameras in the future.

References

ALTER, F., MATSUSHITA, Y., AND TANG, X. 2006. An intensity similarity measure in low-light conditions. In *ECCV (4)*, 267–280.

BAONE, G. A., AND QI, H. 2006. Demosaicking methods for multispectral cameras using mosaic focal plane array technology. *Proc. SPIE 6062*.

BAYER, B. 1976. Color imaging array. *US Patent 3,971,065* (July).

CAO, H., AND KOT, A. C. 2008. A generalized model for detection of demosaicing characteristics. In *ICME*, 1513–1516.

DRAGO, F., MYSZKOWSKI, K., ANNEN, T., AND CHIBA, N. 2003. Adaptive logarithmic mapping for displaying high contrast scenes. *Computer Graphics Forum 22*, 419–426.

FREEMAN, T. W. 1988. Median filter for reconstructing missing color samples. *US Patent 4,724,395*.

GINDELE, E., AND GALLAGHER, A. 2002. Sparsely sampled image sensing device with color and luminance photosites. *US Patent 6,476,865* (Nov).

GUNTURK, B. K., MEMBER, S., ALTUNBASAK, Y., MEMBER, S., AND MERSEREAU, R. M. 2002. Color plane interpolation using alternating projections. *IEEE Trans. Image Processing 11*, 997–1013.

GUNTURK, B., GLOTZBACH, J., ALTUNBASAK, Y., SCHAFER, R., AND MERSEREAU, R. 2005. Demosaicking: color filter array interpolation. *Signal Processing Magazine, IEEE 22*, 1, 44 – 54.

HAMILTON, J., AND ADAMS, J. 1997. Adaptive color plane interpolation in single sensor color electronic camera. *US Patent 5,629,734*.

HIRAKAWA, K., AND WOLFE, P. 2008. Spatio-spectral color filter spatio-spectral color filter array design for optimal image recovery. *IEEE TIP 17*, 10.

KUMAR, M., MORALES, E., ADAMS, J., AND HAO, W. 2009. New digital camera sensor architecture for low light imaging. *IEEE ICIP*.

LANGFELDER, G., ZARAGA, F., AND LONGONI, A. 2009. Tunable spectral responses in a color-sensitive cmos pixel for imaging applications. *Electron Devices, IEEE Transactions on 56*, 11, 2563 –2569.

LI, X. 2005. Demosaicing by successive approximation. *IEEE Trans. Image Process. 14*, 3, 370379.

LU, W., AND TAN, Y. 2003. Color filter array demosaicking: New method and performance measures. 1194–1210.

LUKAC, R. 2008. *Single-Sensor Imaging: Methods and Applications for Digital Cameras*. CRC Press.

MOHAN, A., RASKAR, R., AND TUMBLIN, J. 2008. Agile spectrum imaging: Programmable wavelength modulation for cameras and projectors. *Computer Graphics Forum 27*, 2, 709–717.

RATNER, N., AND SCHECHNER, Y. Y. 2007. Illumination multiplexing within fundamental limits. *Computer Vision and Pattern Recognition, IEEE Computer Society Conference on 0*, 1–8.

SCHECHNER, Y. Y., NAYAR, S. K., AND BELHUMEUR, P. N. 2007. Multiplexing for Optimal Lighting. *IEEE Transactions on Pattern Analysis and Machine Intelligence 29*, 8 (Aug), 1339–1354.

SHOGENJI, R., KITAMURA, Y., YAMADA, K., MIYATAKE, S., AND TANIDA, J. 2004. Multispectral imaging using compact compound optics. *Opt. Exp.*, 16431655.

SUSANU, G., P. S. N. F. C. A. C. P. 2009. Rgbw sensor array. *US Patent 2009/0,167,893* (July).

YAMAGAMI, T., SASAKI, T., AND SUGA, A. 1994. Image signal processing apparatus having a color filter with offset luminance filter elements. *US Patent 5,323,233* (June).

YASUMA, F., MITSUNAGA, T., ISO, D., AND NAYAR, S. 2008. Generalized Assorted Pixel Camera: Post-Capture Control of Resolution, Dynamic Range and Spectrum. Tech. rep., Nov.

Appendix

Our signal-to-noise ratio analysis is inspired by prior work on illumination multiplexing [Schechner et al. 2007]. To capture the effect of the illumination from a single light source in a scene lit by multiple lights, images can be captured by illuminating the scene with each light source at a time. However, this leads to considerable noise due to the low illumination, especially in shadow and occluded regions. [Schechner et al. 2007] shows that acquiring images with multiple multiplexed lights reduces the effect of noise. The effect of each light source can then be recovered by demultiplexing the captured values. The scenario with cameras is analogous. The primaries of a narrow band camera are designed to capture each of the red, green and blue channels separately. Whereas, the primaries of a broad band camera multiplex these bands to improve the light efficiency. Hence, we propose a similar paradigm for analyzing the SNR of different multiplexed or non-multiplexed capture modes in different scene lighting conditions.

Modeling SNR: Let us consider a color basis with n channels whose spectral transmittance overlaps minimally (e.g. RGB). Let the total number of photons reaching the camera from a spatial point before being filtered by the primaries be α. Hence, α changes spatially with the scene content and also with the change in aperture or shutter speed of the camera. For a general camera, let us assume m physical color filters which multiplex these n channels during capture by transmitting or blocking each channel completely (e.g. a cyan primary transmits B and G but blocks R). Let the transmittance of these m primaries be given by $T = (t_1, t_2, \ldots, t_m)^T$. If we assume that the light coming in is evenly distributed across all wavelengths, then the expected value of the amount of light passing through any primary is given by αT. Let us now consider a $m \times n$ multiplexing matrix M such that $M(i, j)$ is 1 if channel i, $1 \leq i \leq n$, is passed and 0 otherwise. Hence, the expected values computed for each channel i, c_i, is given by $E(c_i) = \alpha M_i^{-1} T$, where M_i^{-1} is the ith row of M^{-1}. We define the expected value $E(C)$ of the vector $C = (c_1, \ldots, c_n)$ to be a vector given by $E(C) = (E(c_1), \ldots, E(c_n))$.

There are several sources of noise in any imaging pipeline. For the sake of simplicity we assume the noise level is always computed for the same sensor gain, i.e. ISO number. The sources of noise can be categorized into signal-dependent or signal-independent noise [Schechner et al. 2007; Alter et al. 2006; Ratner and Schechner 2007]. The signal dependent noise can be expressed as a Poisson distribution of the photons that reach the sensor, i.e. each pixel. Since this is dependent on the number of photons, it is the dominant noise when the number of photons is high, i.e. for lighted scenes. The variance of the signal dependent noise for each primary j is therefore proportional to the expected captured values αt_j. Finally, we assume the variance of this signal independent noise is the same across all the primaries, S.

Hence the total variance for channel i is given by $\sigma_i^2 = \sum_{j=1}^{m} (M_{ij}^{-1})^2 (\alpha t_j + S)$. For dark scenes, the signal independent noise dominates and the above equation becomes $\sigma_i^2 = \sum_{j=1}^{m} (M_{ij}^{-1})^2 S$. For bright scenes, on the other hand, the signal dependent noise dominates and the above equation becomes $\sigma_i^2 = \sum_{j=1}^{m} (M_{ij}^{-1})^2 \alpha t_j$. Now, we define the total variance for C as a vector $\sigma_C = (\sigma_i, \ldots, \sigma_n)$. Hence, the signal to noise ratio for C is given by

$$SNR(C) = \frac{|E(C)|}{|\sigma_C|} \tag{3}$$

However, note that defining the SNR for the intensity image g obtained by adding the captured values from the m filters is much simpler. In this case, $E(g) = \alpha \sum_{i=1}^{m} t_i$ and the $\sigma_g = \sqrt{\sum_{i=1}^{m} S + \alpha t_i}$. For dark scenes, $\sigma_g = \sqrt{\sum_{i=1}^{m} S}$, and for bright scenes, $\sigma_g = \sqrt{\sum_{i=1}^{m} \alpha t_i}$ Hence, the $SNR(g) = \frac{E(g)}{\sigma_g}$.

For any camera, we usually know the matrix M^{-1}. For example, the matrix M for an RGB camera is a 3×3 identity matrix since the channels and the filters are identical. Hence, M^{-1} is also identity. But, for CMY cameras with that capture multiplexed RGB channels, the matrix M and M^{-1} are as follows.

$$M_{CMY} = \begin{pmatrix} 0 & 1 & 1 \\ 1 & 0 & 1 \\ 1 & 1 & 0 \end{pmatrix}, \; M_{CMY}^{-1} = \frac{1}{2} \begin{pmatrix} -1 & 1 & 1 \\ 1 & -1 & 1 \\ 1 & 1 & -1 \end{pmatrix} \tag{4}$$

Or, when considering the 5-primary mode of our camera, $n = 5$ since we can capture 5 almost non-overlapping color channels as shown in Figure 3(d). However, $m = 6$. This means that M is not a square matrix, but a 6×5 matrix and M^{-1} is a non-unique pseudo-inverse. M and one such pseudo inverse are shown below.

$$M = \begin{pmatrix} 1 & 0 & 0 & 0 & 0 \\ 0 & 0 & 1 & 0 & 0 \\ 0 & 0 & 0 & 0 & 1 \\ 0 & 0 & 1 & 1 & 1 \\ 1 & 0 & 0 & 0 & 1 \\ 1 & 1 & 1 & 0 & 0 \end{pmatrix} \; M^{-1} = \begin{pmatrix} 1 & 0 & 0 & 0 & 0 & 0 \\ -1 & -1 & 0 & 1 & 0 & 0 \\ 0 & 1 & 0 & 0 & 0 & 0 \\ 0 & -1 & -1 & 0 & 1 & 0 \\ 0 & 0 & 1 & 0 & 0 & 0 \end{pmatrix} \tag{5}$$

Further, note that when computing the ratios of the SNRs of two cameras (for e.g. RGB and CMY) for dark or bright scenes, for both $SNR(C)$ or $SNR(g)$, we do not need to know either α or S since they cancel out. So, as long as we know the transmittance of the primaries Figure 3, we can easily predict the relative improvement or degradation of SNR. Since we know the exact transmittance of the primaries in our camera, we use this to predict two ratios, $\frac{SNR_{CMY}}{SNR_{RGB}}$ and $\frac{SNR_{CMY}}{SNR_{RGBCY}}$, for both bright and dark scenes (Table 1).